University of Oxford

DTC Project Report 2013

Project 1

# Predicting Global Radiation Damage: Improving Beam Profile Measurements and Parameterising a Dose Decay Model

*Author:*
Jonathan Brooks-Bartlett

*Supervisor:*
Prof. Elspeth Garman

July 19, 2013

**Abstract**

During macromolecular X-ray crystallography experiments crystals suffer radiation damage which detrimentally affects the quality of the data that are collected and can lead to incorrect biological interpretations being made. It is thus highly desirable to be able to understand and predict how the extent of the damage affects the observed data. The progression of radiation damage is thought to be proportional to the absorbed dose within the crystal and hence accurate dose measurements and calculations are crucial in understanding the phenomenon of radiation damage.

This report sets out to parameterise a model for the relative diffraction efficiency (RDE) for crystals at cryotemperatures and compare this model with existing experimental data to check whether the model is consistent with other observations. The work reported also aims to improve X-ray beam profile measurements taken with a $10\mu m$ diameter circular aperture at the Diamond Light Source (DLS) synchrotron which can be used to make more accurate dose calculations in the dose calculation software RADDOSE 3D.

The results from the X-ray beam profile experiments carried out in collaboration with Dr. Carina Lobley on DLS beamline I02, suggested that the measured Full Width at Half Maximum (FWHM) is actually closer to the true value of the FWHM then subtracting $5\mu m$ as suggested as a potential correction. It was also found that fitting the X-ray beam flux data to a Gaussian distribution is not always the best approach. Further to this, the experiments highlighted further information about the nature of the X-beam on I02 and showed that it seems to converge as it approaches the position of the crystal sample, which motivates further investigation into this area.

With regards to the RDE model, it was found that the parameterisation obtained gave very promising results for the majority of the experimental data available and it was consistent with experimental observations seen by other researchers for crystals held at cryotemperatures.

The next step of this work is to investigate how the RDE model affects the diffraction weighted dose (DWD) calculations, and whether the DWD is a good measure of the extent of global radiation damage.

# Contents

**1 Introduction** **4**

**2 X-ray Beam Profile Measurements** **5**
- 2.1 Experimental Measurements of the X-ray Beam Flux . . . . . 5
- 2.2 Deconvolving the Beam Measurements . . . . . 6
- 2.3 Implementing the Deconvolution . . . . . 7
- 2.4 Results . . . . . 11
  - 2.4.1 Predicting the FWHM . . . . . 11
  - 2.4.2 Total Flux Measurements . . . . . 11
  - 2.4.3 Fitting Gaussian and Cauchy-Lorentz distributions to Flux Measurements . 11
  - 2.4.4 Further Investigation . . . . . 13

**3 Parameterisation of Relative Difrraction Efficiency Model** **14**
- 3.1 Deriving the RDE Model . . . . . 14
  - 3.1.1 Average Reflection Intensity . . . . . 14
  - 3.1.2 Dose Dependence of the B-factor and the Scale Factor . . . . . 15
  - 3.1.3 Integrated Reflection Intensity and RDE Model . . . . . 15
- 3.2 Calculation of Parameters for the RDE Model . . . . . 15
  - 3.2.1 Experimental Data from Protein Crystals at Cryotemperatures . . . . . 15
  - 3.2.2 Obtaining the Parameters . . . . . 15
  - 3.2.3 Comparison of RDE Model with Results from Owen *et al.* (2006) . . . . . 16
- 3.3 Results . . . . . 16

**4 Discussion** **19**

**Appendices** **21**

**A Difference in FWHM of Convolved measurements and Deconvolved measurements** **21**

**B Derivation of Maximum Likelihood Estimate for a Binomial Distribution** **23**

# 1 Introduction

Radiation damage is one of the major limiting factors for crystallographers when collecting diffraction data in macromolecular X-ray crystallography (MX) experiments [4]. As global radiation damage progresses during an MX experiment, the intensity of the spots seen on the detector decreases [6]. This effect is more pronounced for the high-angle spots that correspond to high resolution data. This degradation of data quality can potentially lead to biological misinterpretations and incorrect protein structures being determined. To mitigate the risk of collecting bad quality data, crystallographic data are often collected at cryotemperatures (100K) because the rate of global radiation damage is dramatically reduced at 100K compared to room temperature (RT) [10]. However, highly intense X-ray beams from synchrotron sources mean that radiation damage can still be a problem at cryotemperatures.

The earliest investigation into the effects of global radiation damage was in 1962 by Blake and Phillips [1] in which they measured the diffracted intensity decay for a particular set of reflections of sperm-whale myoglobin at RT for 300 hours. In their investigation they concluded that the global radiation damage was proportional to the dose absorbed by the crystal, where the dose is defined as the energy absorbed per unit mass.

Since then many other researchers have investigated the effects of global radiation damage and have extended the original model proposed by Blake and Phillips. A detailed account of these developments can be found in the literature (Southworth-Davies et al. 2007 [14]) and the reader is referred here for more information on the topic.

Since it has been proposed that global radiation damage is proportional to the dose absorbed by the crystal it is generally accepted that the dose is a good indicator of the extent of the radiation damage. RADDOSE( [9] [12]) is a software program that is used to compute this dose and more recently RADDOSE-3D( [16]) has been released which can calculate a full temporally and spatially resolved three-dimensional model of the dose distribution throughout a crystal. Two problems arise here. First, to calculate the dose distribution within a crystal, RADDOSE needs to be provided with the X-ray beam profile. This means that the accuracy of the dose distribution provided by RADDOSE is limited by the accuracy of the measurements of the X-ray beam profile that are supplied to the program. Currently the measurements of the beam flux at Diamond Light Source (DLS) beamline I02 are convolved with the $10\mu m$ aperture used to make the measurements, and hence the accuracy of the full width at half maximum (FWHM) calculation is uncertain, and users are currently advised to consider subtracting an amount of $5\mu m$ from the observed FWHM. Secondly, despite being able to calculate a full dose distribution within a crystal, a single summary dose statistic that faithfully represents the overall dose state of the crystal has not yet been established.

With regard to the beam profile measurements, the first half of this report describes the method used to deconvolve the X-ray beam flux data and provide more spatially accurate flux measurements, as well as to extract the FWHM maximum from the data. Since the design of the source code allows RADDOSE-3D to handle any experimental beam profiles, the results of beam profile measurement experiments can immediately be passed and used in the RADDOSE-3D software.

The problem of providing an adequate summary dose statistic is currently being tackle and various dose statistics have been explored with notable ones being 'average dose', '95% threshold average dose' and the 'maximum dose'. A thorough explanation of the attributes of these dose statistics is given in Zeldin 2012 [15]. In Oliver Zeldin's D.Phil thesis he investigates the relationship between the various dose statistics and the relative diffraction efficiency (RDE). In this investigation he found that none of the above dose statistics give a faithful representation of the damage state of the crystal.

In unpublished work, Oliver Zeldin developed a new dose statistic that seems to be a good representation of the damage state of the crystal. The dose statistic, called the Diffraction Weighted Dose (DWD), considers the effective average dose that is observed in the diffraction pattern as opposed to the dose that has been absorbed by the crystal at a given image number. The DWD

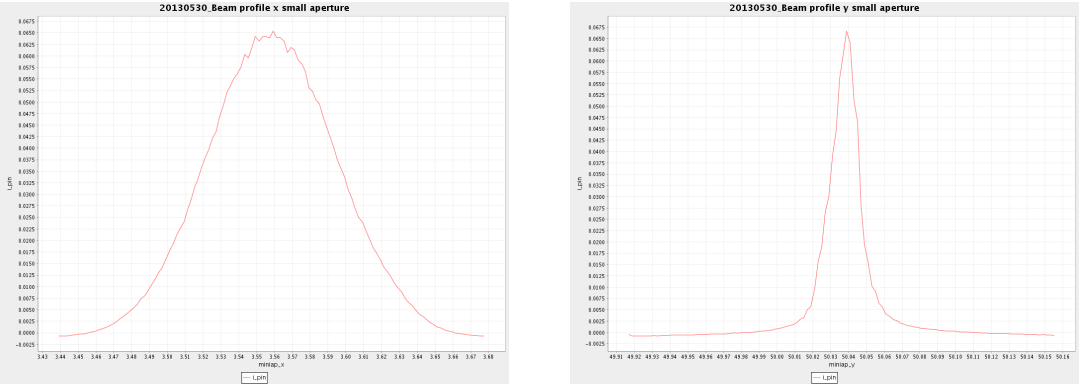


(a) (b)

Figure 1: Examples of the flux measurement data collected at the Diamond Light Source synchrotron. Figure 1a: data collected in the $x$-direction and Figure 1b: data collected in the $y$-direction. The horizontal axis represents the aperture position in millimetres and the vertical axis represents the beam flux intensity in arbitrary units.

is defined mathematically as

$$DWD^i = \frac{\int_{\varphi_{i-1}}^{\varphi_i} \mathrm{d}\varphi \iiint_{crystal} \mathrm{d}x D(\mathbf{x},\varphi) F(\mathbf{x},\varphi) \eta(D(\mathbf{x},\varphi))}{\int_{\varphi_{i-1}}^{\varphi_i} \mathrm{d}\varphi \iiint_{crystal} \mathrm{d}x F(\mathbf{x},\varphi) \eta(D(\mathbf{x},\varphi))} \tag{1}$$

where $\varphi$ is the angle of the rotation axis (the experimental coordinate - proportional to time), $\mathbf{x}$ is the position in the crystal, $D(\mathbf{x},\varphi)$ is the total cumulative absorbed dose (MGy), $F(\mathbf{x},\varphi)$ is the flux density (photons per unit area per radian) and $\eta(D(\mathbf{x},\varphi))$ is the relative diffraction efficiency (RDE), a function of dose which returns the current diffraction efficiency as a fraction of the initial diffraction efficiency (i.e. the relative diffraction intensity given its absorbed dose).
The form of $\eta(D(\mathbf{x},\varphi))$ has not as yet been determined. In the second half of this report the development of a model for $\eta(D(\mathbf{x},\varphi))$ for cryotemperature crystals is discussed and I explain how I determine if the model is consistent with experimental data.

# 2 X-ray Beam Profile Measurements

## 2.1 Experimental Measurements of the X-ray Beam Flux

X-ray beam flux measurements were carried out in collaboration with Dr. Carina Lobley on the DLS I02 beamline. To take experimental measurements of the beam flux at the beamline, scientists use a miniap device which is a piece of steel with a $10\mu m$ diameter circular hole cut into it, which they move across the beam by remote control from outside the experiment hutch. The sample measurement is taken from a diode known as i_pin which is a small diode on the detector shutter, so it measures the number of photons passing through the optics and the sample position on to the detector.
First the 'centre' $x$ and $y$ translation for the aperture is found so that in that centre position the highest beam flux is recorded. The aperture is then translated by $-120\mu m$ and then is scanned across the beam in $2\mu m$ steps until it gets to a position of $+120\mu m$ from the centre. This is carried out both the $x$ and $y$ directions and at each step the diode measurement is recorded. Example of the measurements taken can be seen in Figure 1.

## 2.2 Deconvolving the Beam Measurements

Since the diode measurements are taken every $2\mu m$ in both the $x$ and $y$ directions, it is possible to manipulate experimental measurements to calculate the flux to a spatial resolution of $2\mu m$ despite the aperture size being $10\mu m$ in diameter. The area of the aperture is $(10\mu m/2)^2 \times \pi \approx 78.54\mu m^2$ which means that each diode reading is a convolution of the flux from the space surrounding the central point (see Figure 2).

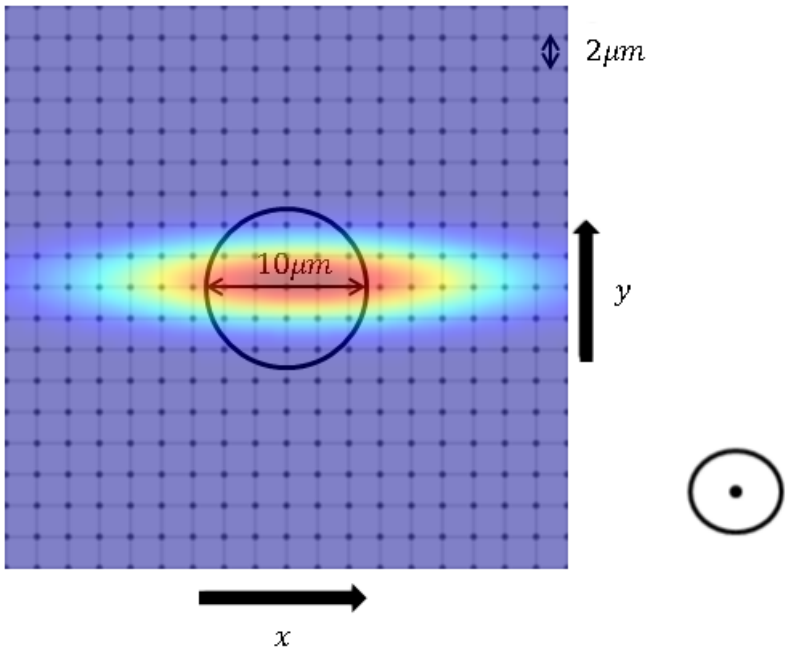


Figure 2: A model of the beam and aperture setup as viewed from the detector looking into the beam. Each point represents a spatial position where a beam measurement is taken, hence the distance between any two horizontally or vertically consecutive spots is $2\mu m$. The circle represents the circular aperture which has a $10\mu m$ diameter. The colour represents the beam flux intensity (not to scale): red is where the intensity is largest and blue is where the intensity is zero. The beam is narrower in the $y$ direction than it is in the $x$ direction. This diagram clearly shows that a reading at a particular point in space is going to be a sum of all of the surrounding points within the aperture area. This means the reading of the total X-ray beam profile that is measured is a convolution of readings from local surrounding space.

Mathematically the convolution between two functions $f(t)$ and $g(t)$ where $t$ is any independent variable is defined as

$$[f * g](t) = \int_0^t f(u)g(t-u)\mathrm{d}u. \tag{2}$$

In our case we can effectively view $f$ as the actual X-ray beam flux, $g$ as the aperture and $[f * g]$ as the measured flux reading. So the problem stated mathematically is given that $[f * g]$ and $g$ are known, can equation 2 be inverted so that $f$ can be found? To do this the convolution theorem [7] can be used which states that

$$\mathscr{F}[f * g] = \mathscr{F}[f]\mathscr{F}[g], \tag{3}$$

where $\mathscr{F}$ denotes the Fourier transform of its argument and the Fourier transform is defined as

$$\mathscr{F}[f(x)](k) = \int_{-\infty}^{\infty} f(x)e^{ikx}\mathrm{d}x. \tag{4}$$

The convolution theorem states that the transformation of the convolution of two functions into Fourier space is equivalent to multiplying the two functions in Fourier space. This provides a way

of finding $f$ without having to invert the integral in equation 2. Thus the true X-ray beam profile denoted $f$ can be found easily by rearranging equation 3 and transforming back to real space giving

$$f = \mathscr{F}^{-1}\left[\frac{\mathscr{F}[f * g]}{\mathscr{F}[g]}\right], \tag{5}$$

where $\mathscr{F}^{-1}$ is the inverse Fourier transform defined as

$$f(x) = \frac{1}{2\pi}\int_{-\infty}^{\infty} \mathscr{F}[f(x)](k)e^{-ikx}\mathrm{d}k. \tag{6}$$

Equation 5 is known as an inverse filter in signal processing and analysis and this equation is relatively easy to evaluate. However, its drawback is that it does not take into account any noise that is introduced in the measurements. In reality the problem is not likely to be of the form given by equation 2, but instead it is more likely to be of the form

$$[f * g](t) = \int_0^t f(u)g(t-u)\mathrm{d}u + n(t), \tag{7}$$

where $n$ denotes noise in the system. Clearly the standard inverse filter is not applicable in the situation where noise is present, but a solution for this case would be to use a Wiener Filter which is a filter that attempts to remove noise as well as restore the original flux signal through minimising the mean-squared error between the true deconvolved flux signal and the calculated deconvolved flux signal. The Wiener Filter, $W$, is defined mathematically in the Fourier domain as:

$$W = \frac{1}{\mathscr{F}(g)}\left[\frac{|\mathscr{F}(g)|^2}{|\mathscr{F}(g)|^2 + \frac{\mathscr{F}(n)}{\mathscr{F}(f)}}\right]. \tag{8}$$

Notice that the Wiener filter contains a term that looks similar to the inverse of a signal to noise ratio in the Fourier domain. If this value is known exactly then the Wiener filter often works really well although it is more common that the value of that ratio is unknown, and it is often treated as a constant value throughout the domain which is being estimated.
The Wiener filter is multiplied with the convolved function in the Fourier domain to give

$$\mathscr{F}[\widehat{f}] = W\mathscr{F}[f * g], \tag{9}$$

such that $\mathscr{F}[\widehat{f}]$ is the solution found with the minimum mean squared error with the true solution $\mathscr{F}[f]$, denoted

$$\text{error} = E\left[\left(\mathscr{F}[f] - \mathscr{F}[\widehat{f}]\right)^2\right]. \tag{10}$$

Parseval's theorem implies that minimising the mean squared error in the Fourier domain is equivalent to minimising the mean squared error in the real domain. For further details on the Wiener Filter and its formal derivation the reader is referred to [5].

## 2.3 Implementing the Deconvolution

In this section the deconvolution of the data is briefly outlined and verification of the accuracy of the solution is presented. The deconvolution algorithm was implemented in Matlab R2012a. First the initial diode measurements were read into Matlab and I fitted the data to a one-dimensional Gaussian function to obtain the parameters for a best fit in both the $x$ and $y$ directions (see Figure 3). The parameters obtained were then used in the formula for a two-dimensional Gaussian function

$$g(x,y) = A_{max}\exp\left[-\left(\frac{(x-\mu_x)^2}{2\sigma_x^2} + \frac{(y-\mu_y)^2}{2\sigma_y^2}\right)\right], \tag{11}$$

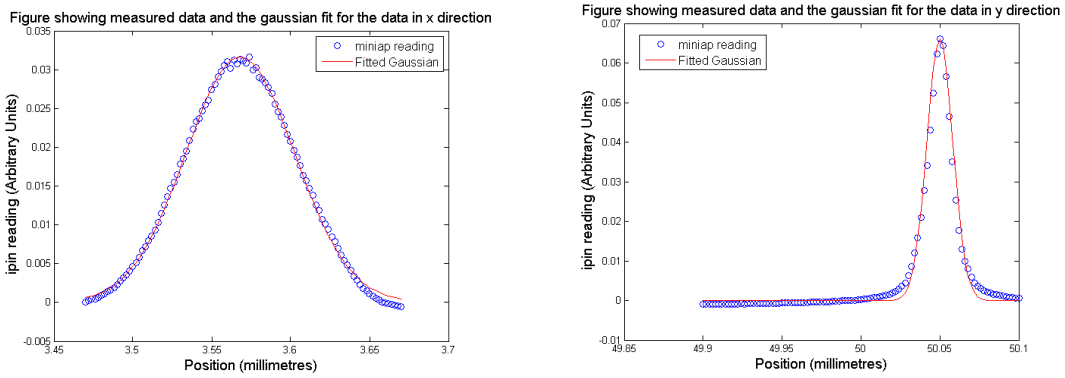


(a) (b)

Figure 3: The original miniap readings from the $10\mu m$ diameter aperture are shown as blue circles and the solid red is the Gaussian fit to the data. Figure 3a: beam profile in the $x$-direction and Figure 3b: beam profile in the $y$-direction.

where $\mu_x$, $\mu_y$, $\sigma_x$ and $\sigma_y$ are the parameters obtained from fitting the one-dimensional Gaussian functions

$$g(x) = A_x \exp\left[-\frac{(x-\mu_x)^2}{2\sigma_x^2}\right], \tag{12}$$

$$g(y) = A_y \exp\left[-\frac{(y-\mu_y)^2}{2\sigma_y^2}\right], \tag{13}$$

and $A_{max}$ is the maximum value of $A_x$ and $A_y$ which are the values of the maximum recorded diode measurement in the $x$ and $y$ directions respectively. If the measurements are taken perfectly (i.e. aperture is scanned exactly across the maximum flux in $x$ and $y$) then $A_x = A_y$ but due to experimental error this is rarely the case.
Equation 11 gives the entire (convolved) two-dimensional beam profile which has to be deconvolved with a smaller matrix that corresponds to convolving with the correct aperture size. The aperture matrix is found by creating a square matrix with the minimum area required to contain all of the points measured for an aperture of a given diameter. Each point in that matrix is then given the value of the Euclidean distance away from the centre point. Any points with a Euclidean distance smaller than the aperture radius is within the aperture area and is given the value 1 (so it contributes to the convolved signal), the rest are given the value zero.
The signal to noise ratio type term in equation 8 is estimated using a minimisation function in Matlab called '*fminsearch*' which returns the value of the parameter that minimises the value that is returned by an objective function. Thus I wrote an objective function that takes in an estimate for the signal to noise ratio and deconvolves the signal using the two-dimensional beam profile and the aperture matrix. The function then convolves the deconvolved signal with the same aperture matrix and calculates the 2-norm (i.e. the square root of the maximum eigenvalue of a matrix multiplied by its conjugate transpose) of the original convolved signal subtracted from the newly calculated convolved signal. This 2-norm value is returned by the objective function. If the two signals give a norm value of zero then they are exactly the same, otherwise a positive value is returned. The *fminsearch* algorithm returns the value of the signal to noise ratio term that minimises the objective function. Given the convolved two-dimensional beam profile, the aperture matrix and the signal to noise ratio, the beam profile can be deconvolved using the Matlab function '*deconvwnr*' which performs a Wiener deconvolution as described in section 2.2 (see Figure 4).
The deconvolved two-dimensional beam profile will not be very smooth because the process of deconvolution is not a straight forward operation and so a Gaussian fit is applied to the deconvolved data in order to obtain a smooth beam profile. This is carried out by taking one-dimensional slices

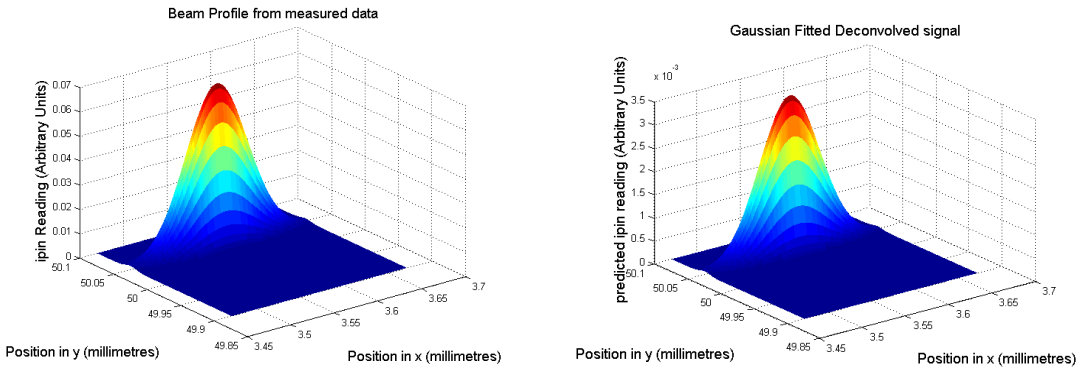


(a) (b)

Figure 4: The two-dimensional Gaussian beam profiles. Figure 4a: two-dimensional profile of the convoluted readings and Figure 4b: beam profile after deconvolution and a further Gaussian fit. Notice that the scales on the vertical axes are very different.

of the two-dimensional beam profile in both the $x$ and the $y$ directions around the slice that gives the maximum readings, and then obtaining the parameters as previously outlined above (see Figure 4b). Using the data with the fitted parameters, any properties of the Gaussian beam can be determined. One of the important properties for the DLS to be able to provide to users is the Full Width at Half Maximum (FWHM) of the beam. The FWHM is defined mathematically as

$$FWHM = 2\sigma\sqrt{2\ln(2)}. \tag{14}$$

Finally a prediction of the reading that would be obtained with apertures of a different size was performed. It is necessary to do this because there is not a measuring device available to take measurements at the resolution to which the method attempts to spatially resolve the flux readings. This was simply performed by convolving the two-dimensional (deconvolved) signal with an aperture matrix of a different size and then taking the values from the one dimensional slices that give the maximum readings in the $x$ and $y$ directions. These calculated values could then be compared with the readings taken from experimental data obtained using an aperture of the equivalent size.

It was noticed whilst X-ray flux measurements were being taken that a Gaussian distribution did not always fit the data very well especially for the flux measurements in the $y$ direction, which due to the beamline optics has a much narrower profile than the $x$ direction. Another problem was that some of the experimental measurements were giving negative beam flux values, which is physically unrealistic. Figure 5 illustrates an example where the Gaussian distribution is clearly not a good fit to the data and hence may give inaccurate FWHM values. The longer tails in Figure 5 suggest that another distribution such as the Cauchy-Lorentz distribution might be a more suitable fit to the data. The figure also gives an example where the experimental data gave negative flux values caused by the diode having a negative zero offset.

Using 27 datasets where measurements were taken with an aperture, I tested to see whether the X-ray flux measurements were better fitted with a Gaussian or a Cauchy-Lorentz distribution using a least squares approach. First the raw data to the two distributions was fitted, and then the two distributions to the data where the flux measurements were shifted were fitted so that there were no negative flux readings. One distribution was deemed a better fit than the other if the sum of squares of the residuals was smaller than that of the other.

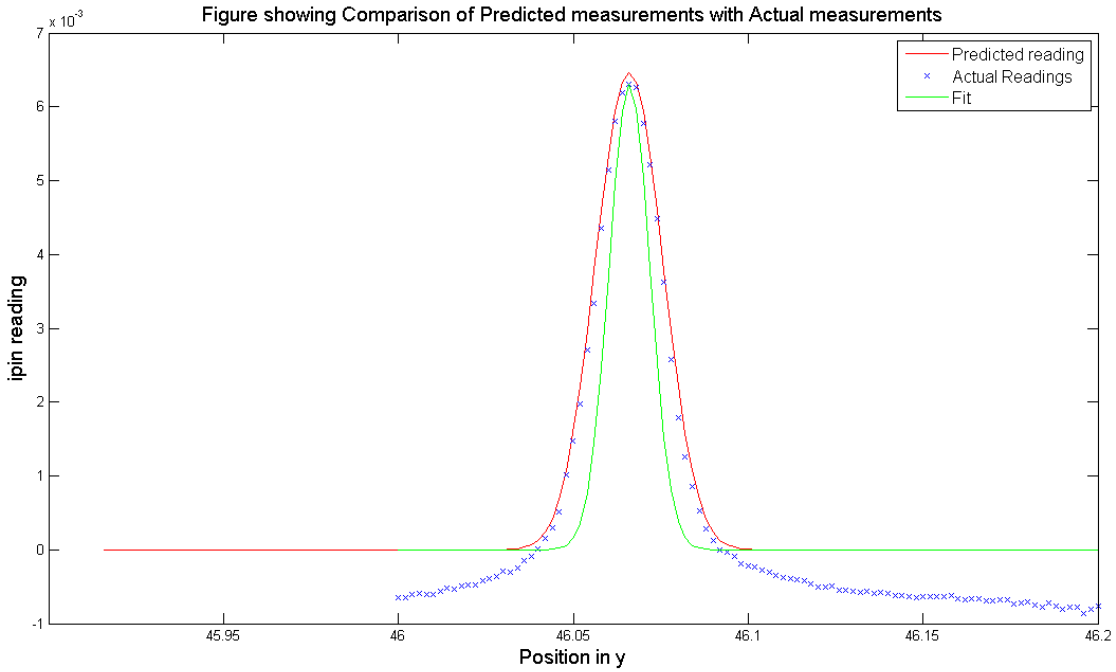


Figure 5: Data on the profile in the $y$ direction obtained during an experimental run where measurements were taken with an aperture with $20\mu m$ diameter aperture. The green solid line shows the Gaussian distribution that was fitted to the experimental data which shown as discrete blue crosses. The red solid line shows the predicted values. The tails on the experimental data do not fit a Gaussian distribution very well and they may better resemble a Cauchy-Lorentz distribution. Another important feature of this figure is the fact that the experimental measurements show negative beam flux values which is physically impossible. This is due to the diode having a negative zero offset.

## 2.4 Results

### 2.4.1 Predicting the FWHM

The RADDOSE user interface requires specific user input regarding the X-ray beam profile with the relevant input parameters here being the beam type (top-hat, Gaussian etc.) and the FWHM. Assuming that the data took the form of a Gaussian distribution, experimentally observed FWHM readings using the $10\mu m$ diameter aperture and deconvolved FWHM predictions were compared. FWHM values obtained from experimental measurements using a $20\mu m$ diameter aperture and the predicted FWHM that was calculated theoretically using a $20\mu m$ diameter aperture were also compared.

Table 1: Table comparing predicted FWHM values with experimentally observed FWHM values

| | FWHM in $x$ | % Error in $x$ | FWHM in $y$ | % Error in $y$ |
|---|---|---|---|---|
| $10\mu m$ diameter aperture experimental measurement | $81.6\mu m$ | 0.49% | $19.5\mu m$ | 4.84% |
| Predicted values of the deconvolved beam profile | $81.2\mu m$ | | $18.6\mu m$ | |
| | | | | |
| Predicted value using $20\mu m$ diameter aperture | $83.9\mu m$ | 2.57% | $22.3\mu m$ | 1.83% |
| Observed value using $20\mu m$ diameter aperture | $81.8\mu m$ | | $21.9\mu m$ | |

Table 1 shows the results from the experiments and the predictions for the FWHM from the measured profiles of the beam. It is noticeable that as the aperture size increases, the measured FWHM also increases. Analysis of the entire dataset showed that the smaller the measured FWHM, the greater the error in the FWHM prediction between that observed with using the $10\mu m$ diameter aperture and the predicted values for the deconvolved beam profile (see appendix A for mathematical explanantion). **These findings suggest that measurements taken with the smallest aperture will give values of the FWHM closest to the true values of the FWHM of the beam and the bigger the true FWHM the smaller the error between the true and measured FWHM**. From the values in table 1, I would advise beamline users to use the FWHM values calculated from the $10\mu m$ diameter aperture measurements and not to subtract $5\mu m$ from the quoted FWHM because doing so will give a much bigger error.

### 2.4.2 Total Flux Measurements

Using the deconvolved flux calculations it was possible to predict the flux readings that would be measured during a wire scan. A wire scan is where a piece of tungsten wire (about $500\mu m$ thick) is moved (remotely) across the beam and flux measurements are recorded sequentially as the wire is moved. The results show that the predicted total flux is very close to the experimentally measured total flux suggesting that the deconvolution algorithm produces a good model for the actual beam profile (see figure 6).

### 2.4.3 Fitting Gaussian and Cauchy-Lorentz distributions to Flux Measurements

During the set of tests in which the raw flux data was used, 22 out of the 27 (81.4%) data sets were better fitted using a Gaussian distribution. However after shifting the data to only contain non-negative values, the number of data sets that were better fitted by a Gaussian distribution dropped to 15 out of the 27 (55.6%).
More interesting are the conditions under which each distribution becomes a better fit. The Gaussian distribution was always a much better fit for the measurements in the $x$ direction (see Figure 7a, whereas for the data sets that were non-negative the Cauchy-Lorentz distribution was always a better fit for the measurements taken in the $y$ direction (see Figure 7b) except when the measurements were taken with a $20\mu m$ diameter aperture instead of $10\mu m$. The FWHM given by the Gaussian distribution in Figure 7b is $20.5\mu m$ however the FWHM given by the Cauchy-Lorentz fit is $16.1\mu m$. This difference of $4.4\mu m$ is quite significant considering the size of the FWHM values

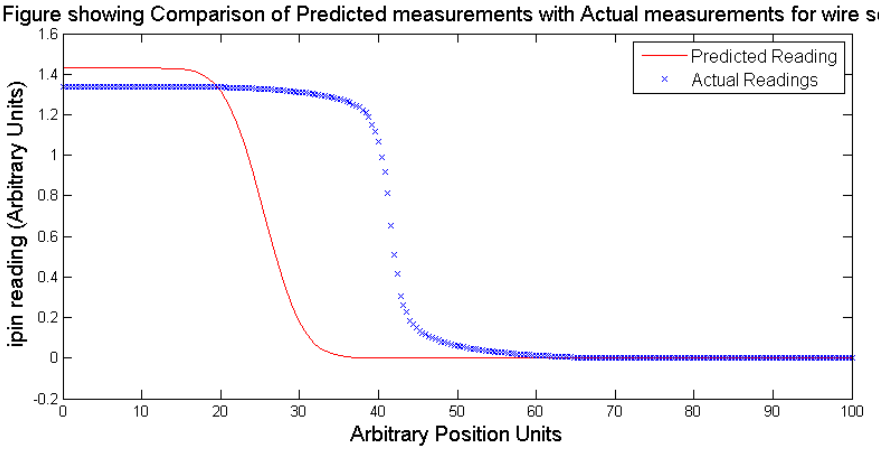


Figure 6: Wire scan taken along the $y$ direction. The solid red line show the predicted flux reading using the deconvolved flux data. The blue crosses measured flux data during the wire scan experiment. The $x$-axis on the plot is completely arbitrary and does not represent the position of the curves relative to one another. It can be seen that the shape of the two curves are very similar and that the total flux measured at position 0 is very similar to the total flux calculated. Some of the discrepancy between the total flux measured and predicted can be explained due to the diode having a negative zero offset (see figure 5)

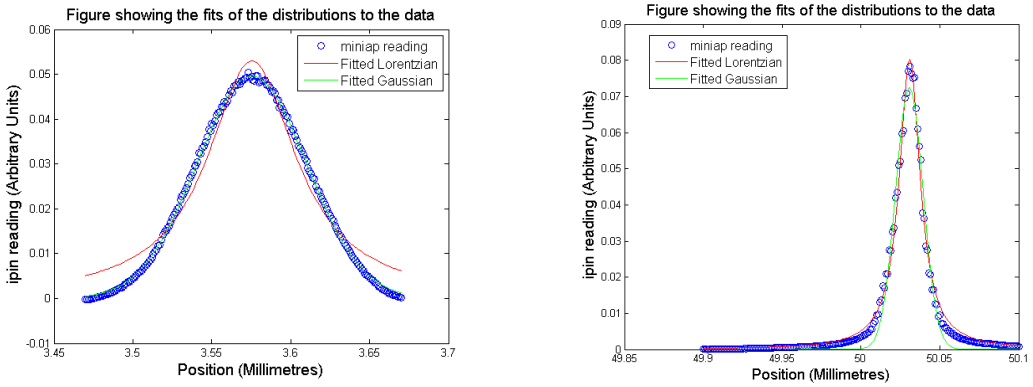


(a) (b)

Figure 7: Comparison between the Gaussian and Cauchy-Lorentz distribution fits to the experimental flux data measurements. Figure 7a: data in the $x$ direction and Figure 7b: data in the $y$ direction. The Gaussian distribution is clearly a better fit in Figure 7a but the Cauchy-Lorentz distribution is a better fit in Figure 7b.

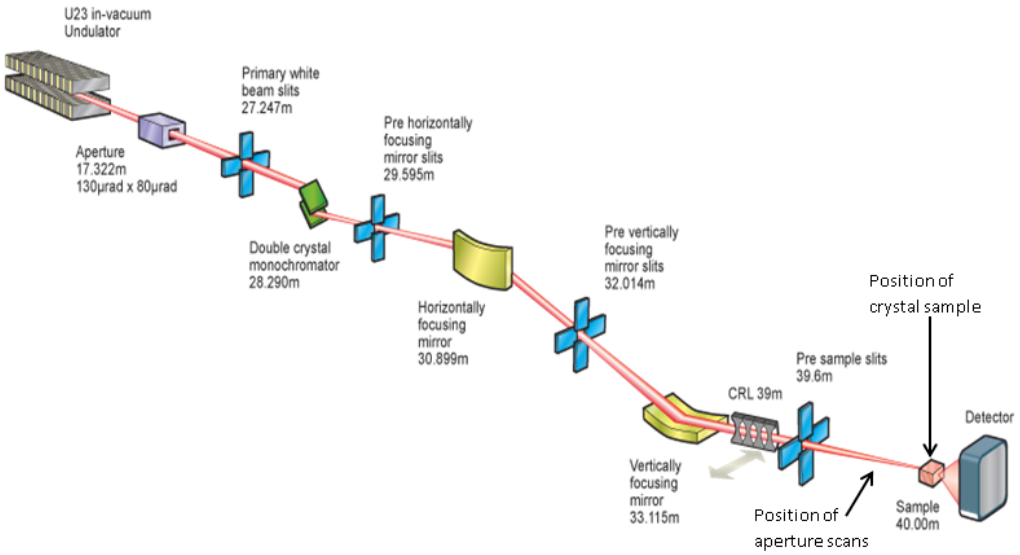


Figure 8: This schematic of the DLS beamline shows some of the important features of the beamline such as the horizontal and vertical focusing slits that change the dimensions of the beam. The position where the routine miniap aperture measurements take place is also shown in this diagram (not to scale). It shows that the miniap scans are taken at a position closer to the X-ray beam source relative to the crystal sample. The results of our experiments showed that the to converges as it travels and hence the FWHM at the location where the routine miniap scans take place are bigger than when measured at the crystal position. This figure was obtained by permission from Dr. Carina Lobley at the DLS.

calculated, so I would suggest that modelling the beam profile as a Cauchy-Lorentz distribution when using a $10\mu m$ diameter aperture in the $y$ direction will actually give more accurate FWHM values than those that are being used by the beamline currently.

### 2.4.4 Further Investigation

Despite the calculation of the FWHM being the main area of concern for this report, the results also provided increasing insight into the nature of the beam profile and the investigation thus raised even more questions. The routine miniap measurements are taken from a different position relative to the mounted crystal sample position (see Figure 8). It was found that taking aperture measurements from the crystal position led to lower flux measurements and smaller FWHM values, (see Figure 9) which suggested that there must be a convergence of the beam which was later confirmed by the principal beamline scientist at the beamline. The convergence was much more pronounced in the $y$ direction than in the $x$ direction which is due to the fact that the vertical beam focussing slits are closer to the sample than the horizontal focussing slits. The smaller flux measurements are currently unexplained. Investigation into the extent to which the beam converges and why the observed flux is smaller at the crystal position would allow better calculations of the flux incident on the crystal and improve the absorbed dose calculations.

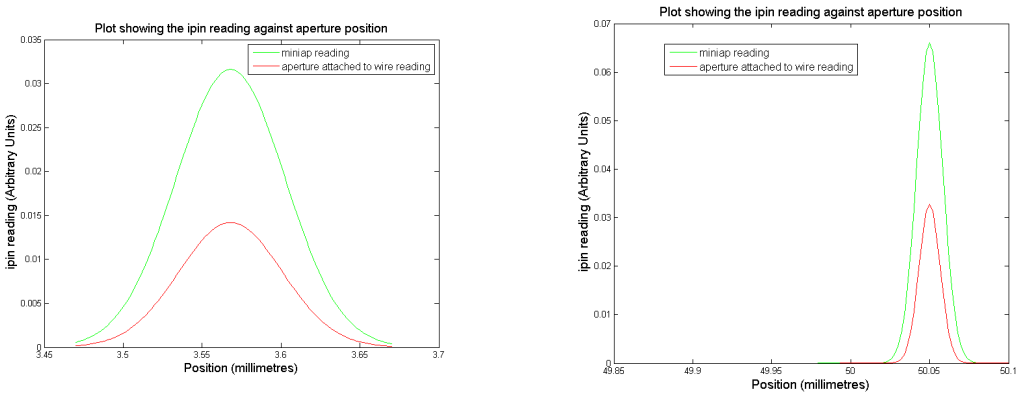


(a) (b)

Figure 9: I-pin reading plotted against the aperture position in the $x$-direction (Figure 9a) and in the $y$-direction (Figure 9b). The measurements with the label "*miniap reading*" were taken with an $10\mu m$ diameter aperture that is in a position closer to the X-ray beam source relative to the data acquired with the label "*aperture attached to wire reading*" which is taken at the position where the crystal sample would be mounted (see Figure 8). It is clear that the flux readings differ quite significantly for the beam in the different positions. The FWHM for the miniap in the $x$-direction is $81.6\mu m$ whereas for the aperture attached to the wire in the $x$-direction the FWHM is $77.0\mu m$. Similarly the FWHM for the miniap in the $y$-direction is $19.5\mu m$ whereas for the aperture attached to the wire in the $y$-direction the FWHM is $15.7\mu m$. This shows that the beam is converging as it travels towards the crystal sample.

# 3 Parameterisation of Relative Difrraction Efficiency Model

## 3.1 Deriving the RDE Model

### 3.1.1 Average Reflection Intensity

In MX experiments the intensity of an observed spot on a diffraction pattern $\mathbf{I}$ is proportional to the square of the structure factor $\mathbf{F}$ and the temperature factor $\mathbf{T}$ [2] and hence can be written as

$$\mathbf{I} = C \times |\mathbf{F}(\theta)|^2 \times \mathbf{T}(\theta), \tag{15}$$

where $C$ is known as the scale factor that takes into account factors such as the incident beam intensity, volume of the crystal and the volume of the unit cell [13] and $\theta$ is the angle of reflection (also known as the Bragg angle).
The temperature factor takes the form $\mathbf{T}(\theta) = \exp\left(-2B\sin^2(\theta)/\lambda^2\right)$ where $\lambda$ is the wavelength of the incident X-ray beam and $B$, known as the B-factor with units $\text{Å}^2$, is related to the mean-square displacement of the atomic vibrations [3], so equation 15 becomes

$$\mathbf{I} = C \times |\mathbf{F}(\theta)|^2 \times \exp\left(\frac{-2B\sin^2(\theta)}{\lambda^2}\right). \tag{16}$$

In [13] Popov and Bourenkov used a statistical approach to estimate the average squared structure factors. Rather than use the reflection angle as the explicit independent variable they instead use the reciprocal distance $h = 2\sin(\theta)/\lambda$ as the independent variable. They also experimentally determine the observed reflection intensity distribution, which will be denoted $\mathbf{J}(h)$, from 72 randomly chosen protein crystals at room temperature (RT). From this experimental distribution it is possible to calculate the expectation value of the squared structure factor magnitudes which will be denoted $\widehat{J}(h) = E[|\mathbf{F}(\theta)|^2]$ where $E[]$ denotes the expected value of its argument. The calculated expectation values of the squared structure-factor magnitudes were provided by Bourenkov but details of the method are provided by Popov and Bourenkov in [13].

### 3.1.2 Dose Dependence of the B-factor and the Scale Factor

With the change in independent variable and the statistical variables adopted in 3.1.1, equation 16 can be written as

$$\mathbf{J}(h) = C \times \widehat{J}(h) \times \exp\left(-\frac{Bh^2}{2}\right), \tag{17}$$

which is the model used by Leal *et al.* [8]. It is important to note the isotropic B-factor approximation is used by Leal *et al.* in the derivation of the integrated reflection intensity. This means that equation 17 only applies to a narrow wedge of data which was specific to their experiments conducted at RT. I am extending this model using data available to see if this model can adequately describe experimental results at cryotemperatures. In Figure 1 of [8], Leal *et al.* show that there is a dose dependence on both the scale factor, $C$, and the B-factor, $B$, in equation 17. They state that the dependence of these parameters on dose can be described by the forms:

$$B(D) = B_0 + \beta D, \tag{18a}$$

$$C(D) = K \exp\left(-\gamma^2 D^2\right), \tag{18b}$$

where $B_0$, $\beta$, $K$ and $\gamma$ are constant parameters to be determined and $D$ denotes the absorbed dose as previously defined in section 1.

### 3.1.3 Integrated Reflection Intensity and RDE Model

In order to calculate the integrated reflection intensities, $I_\Sigma(D)$, equations 17, 18a and 18b can be combined and integrated over $h$, which gives

$$I_\Sigma(D) \propto \exp\left(-\gamma^2 D^2\right) \int_0^{1/d_{min}} h^2 \widehat{J}(h) \exp\left(-\frac{(B_0 + \beta D)h^2}{2}\right) \mathrm{d}h, \tag{19}$$

where $d_{min}$ is the distance corresponding to the distance between Bragg planes in the real space crystal lattice.
The RDE and hence $\eta$ is given by $I_\Sigma(D)/I_\Sigma(0)$.

## 3.2 Calculation of Parameters for the RDE Model

### 3.2.1 Experimental Data from Protein Crystals at Cryotemperatures

In [8] the calculated values for the parameters in equation 19 were determined for 15 different protein crystals at RT but the parameter values quoted for protein crystals at cryotemperature seem to give inconsistent results when I compared them with cryotemperature data collected by Owen *et al.* 2006 [11]. It was therefore necessary to obtain parameter values with experimental data from protein crystals held at cryotemperatures.
The data were collected from an experiment outlined in Zeldin's thesis, in which 16 cubic crystals of bovine pancreatic insulin were tested under three dose contrast regimes. 5 crystals were tested under a *big beam* dose contrast regime where the FWHM of the X-ray beam was approximately $115 \times 115 \mu m^2$, 6 were tested under a *medium beam* dose contrast regime where the beam FWHM was approximately $60 \times 60 \mu m^2$ and 5 crystals were tested under a *small beam* dose contrast regime where the beam FWHM was $25 \times 40 \mu m^2$. The data were collected from each crystal using an initial low-dose *probe* data set and then 10 cycles of *burn* and *probe* where *burn* was a high dose exposure of the crystal to the beam with no data collection during this phase.

### 3.2.2 Obtaining the Parameters

Dividing equation 17 by $\widehat{J}(h)$ and taking the natural logarithm of both sides yields

$$\ln\left(\frac{\mathbf{J}(h)}{\widehat{J}(h)}\right) = \ln(C) - \frac{B}{2}h^2, \tag{20}$$

which is the equation of a straight line where $\ln(C)$ is the intercept and $-\frac{B}{2}$ is the gradient (notice that since $K$ cancels in $I_\Sigma(D)/I_\Sigma(0)$ it is not necessary to find this parameter for the RDE model). Equation 20 gives a single value for each of $C$ and $B$ for a given *probe* and hence for a given dose for each crystal. The dose statistic that is used is the maximum dose since this is the dose value that is returned when using RADDOSE version 2 which was reportedly used for the dose calculations by Leal *et al.* The straight line is fitted using a least squares approach for each *probe* to generate a set of values for each of the parameters $C$ and $B$. Again a least squares approach is used to fit equations 18a and 18b to obtain the parameters $B_0$, $\beta$ and $\gamma$ ($K$ is also calculated) that best reproduce the data for a given crystal. This process is performed for each crystal in a given dose contrast regime and the values of the parameters for each crystal are then averaged, taking the median average value to avoid bias from values that are regarded as outliers.
When applying the method used above, account had to be taken for the fact that the experimental data quoted values for 10 real space resolution bins in the range 5.7Å-1.8Å whereas the calculated expectation values of the squared structure factors (supplied by Bourenkov as previously mentioned) were split into 300 bins in reciprocal space corresponding to a resolution range of 12.0Å-0.9Å. To consolidate this I converted the reciprocal space resolutions bins into real space resolution bins using Bragg's Law, $h = 1/d = 2\sin(\theta)/\lambda$ where $d$ is the distance between Bragg planes, and then grouped the values into the same resolution bins as the ones that were reported for the experimental data. The mean average of the expectation values in each of the newly grouped real space resolution bins is taken, which is the same as was performed on the reported experimental intensity values that were supplied by Zeldin.

### 3.2.3 Comparison of RDE Model with Results from Owen *et al.* (2006)

The 'rate' of global radiation damage appears to be practically the same for every protein crystal at cryotemperatures [6] so we should also expect the RDE model to be consistent with the results seen in Owen *et al. 2006* [11]. Owen *et al.* fitted straight lines to the experimental data for the RDE of (all) seven crystals in the experiment with corresponding correlation coefficient values above 0.95. To test if the RDE model is consistent with the results from [11] I set up a statistical test to see how well a straight line fitted the RDE model after applying some Gaussian noise to simulate experimental error.
A single trial for the test returned a value stating the number of times out of seven that a straight line fitted the data generated by the RDE model with a correlation coefficient of 0.95 or above after applying Gaussian noise. The trial was considered a success if the value returned was seven, otherwise it was deemed a failure. Ten equally spaced data points were simulated between dose values of $0MGy$ between $70MGy$, which is similar to the number of data points and the range for the experiments carried out in [11]. The Gaussian noise was estimated to have mean equal to 0 and a standard deviation equal to 0.0149 which was estimated from the reported error on the experimental dose limit by Owen *et al.* (The experimental dose limit is the value of the dose that reduces the RDE to 0.5, which was found to be $43MGy \pm 3MGy$).
Statistically the results of these trials form a binomial distribution where the probability of observing $k$ successes in $n$ trials is given by

$$P(k; n, p) = \binom{n}{k} p^k (1-p)^{n-k}, \tag{21}$$

where $p$ is the probability of success. The probability of success can be estimated using maximum likelihood estimation. The maximum likelihood estimate of the probability of success for a binomially distributed random variable is quite intuitively the total number of successful trials divided by the total number of trials (see Appendix B for the derivation).

## 3.3 Results

Table 2 shows the parameter values that were calculated for each dose contrast regime. Figure 10 shows plots of the RDE against dose for each of the dose contrast regimes.

Table 2: Table showing the parameter values obtained for the three dose contrast regimes

| Dose Contrast Regime | $B_0$ | $\beta$ | $\gamma$ |
|---|---|---|---|
| *Small Beam* | 12.194 | 0.149 | 0.014 |
| *Medium Beam* | 10.453 | 0.199 | 0.011 |
| *Big Beam* | 16.218 | 0.034 | 0.019 |

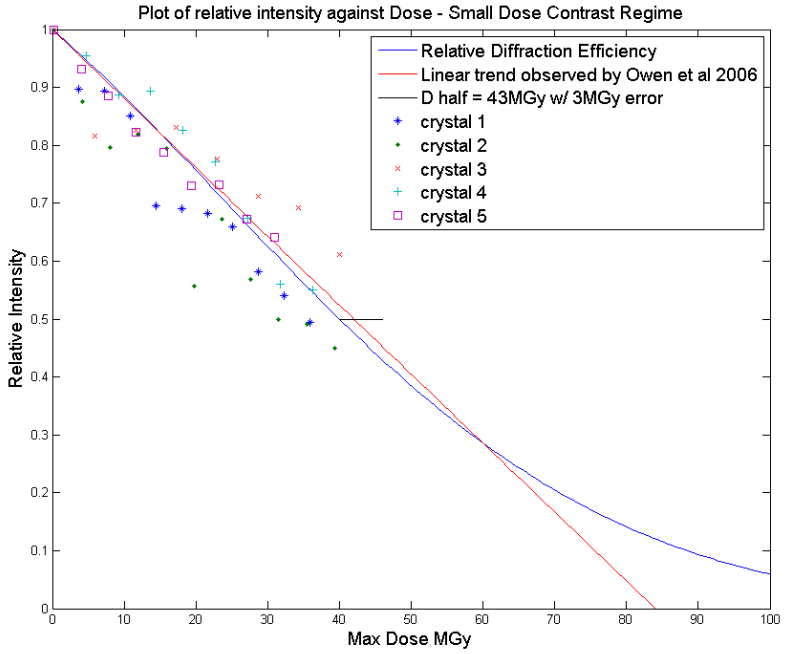


(a)

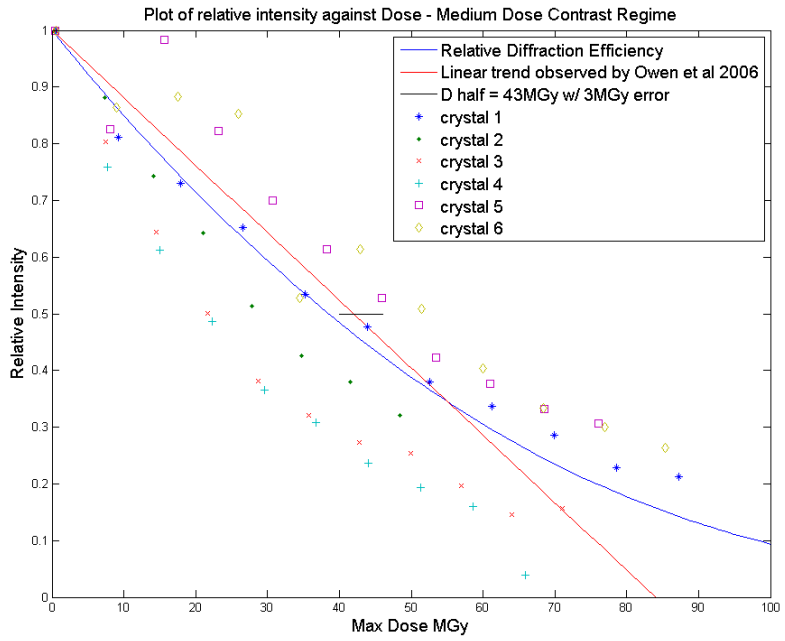


(b)

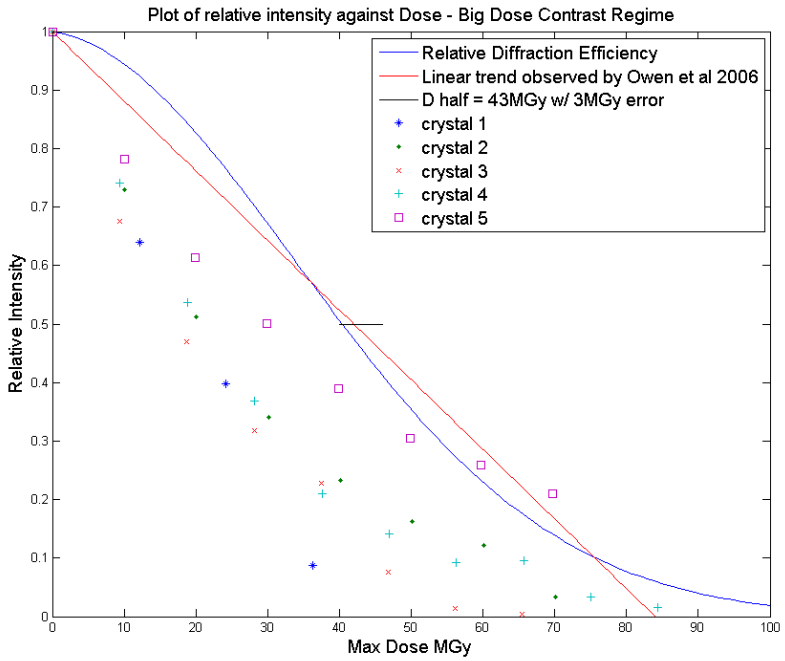


(c)

Figure 10: RDE for each dose contrast regime Figure 10a: *small beam*, Figure 10b: *medium beam*, Figure 10c: *big beam*. The blue solid line shows the RDE using the corresponding parameters from table 2. The solid red line is a straight line that approximates a good fit to the experimental data in Owen *et al.* 2006 and goes through the point $(43MGy, 0.5)$ with the solid black line showing the error reported on the experimental dose limit given in the same paper. The discrete points show the experimental data for each insulin crystal.

On the plots in Figure 10, the solid blue line denotes the RDE using the corresponding parameters from table 2 for the Zeldin data. The solid red line approximates the data measured by Owen *et al.* (2006) where a straight line was an extremely good fit to the data between dose values of $0MGy$ to around $70MGy$ and the experimental dose limit. The discrete points in the plots in Figure 10 represent actual RDE data for each insulin crystal. The RDE model seems to be a good fit for the *small beam* and *medium beam* dose contrast regimes. However for the *big beam* dose contrast regime, the model does not seem to fit the data and the overall shape of the curve looks significantly different from the other two regimes, particularly between the dose values of $0MGy$ to around $40MGy$. This effect could be explained by the results from Zeldin's D.Phil thesis, in which he demonstrates that the maximum dose value (amongst other dose statistics) is not always good at representing the extent of global radiation damage within a crystal.
To test if the RDE model was consistent with the results found by Owen *et al.* (2006) I performed 100 trials as described in section 3.2.3. A maximum likelihood estimate was recorded for the parameter of the probability of success equal to 1 i.e. every trial was successful (see Figure 11). I did this for each of the three sets of parameters for the RDE model and obtained the same result. This means that the RDE model derived above with each set of parameters is consistent with the straight line observations reported by Owen *et al.* for crystals at cryotemperatures.

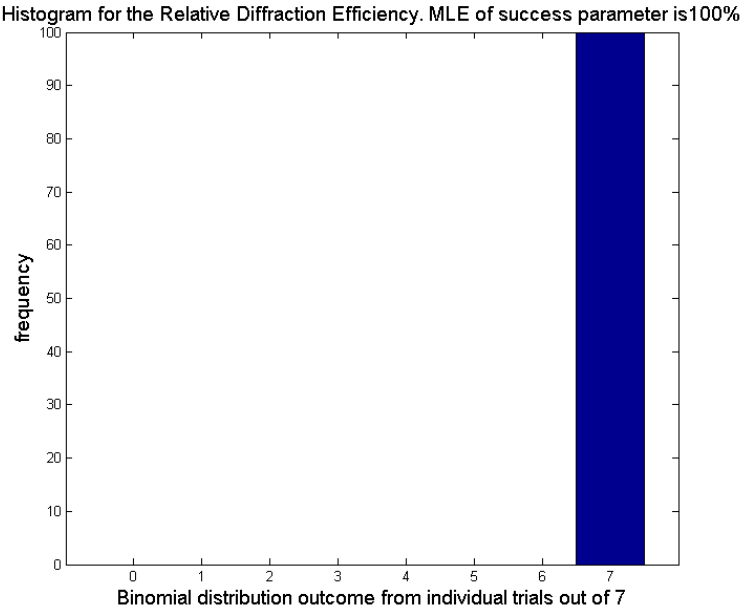


Figure 11: Histogram of the frequency with which a trial recorded a given number of times out of seven when the correlation coefficient value was $\geq 0.95$. The histogram shows that all 100 simulated trials (discussed in section 3.2.3) were successful. Note that only the outcomes recorded that returned the value seven were counted as successes, the rest were considered failures.

# 4 Discussion

We have shown that the FWHM maximum for the X-ray beam profile measured using the $10\mu m$ aperture is a much better estimate of the true FWHM of the beam than subtracting $5\mu m$ and that for a narrower beam, the Cauchy-Lorentz distribution fits the flux data better than a Gaussian.
In the process of collecting the X-ray beam data a further area of investigation was identified regarding the nature of the X-ray beam. The beam converges on the crystal sample and hence the measurements of the beam taken with the miniap are not necessarily spatially accurate values of the flux incident on the crystal sample. Understanding how the beam converges would be essential to provide a more accurate calculation of the flux incident on the crystal during MX experiments on the I02 beamline at DLS. It was also observed that the flux measurements taken at the sample position were smaller than those at the routine apeture position and at present; this phenomenon is unexplained.
It would be beneficial for these sorts of investigations into the X-ray beam behaviour to be carried out on other beamlines so that the X-ray beam profile can be measured more accurately. This would greatly improve the accuracy of the dose distribution calculated in the RADDOSE-3D software, which would allow for much better estimates of the extent of radiation damage within a crystal sample.
The results from the model of the RDE model seem very promising. With appropriate parameters the model has been shown to be applicable to crystals at both RT [8] and at cryotemperatures (presented in this report). The model has also been shown to be consistent with the linear appearance of the relative intensity decay with dose observed by Owen *et al.* [11]. Despite this, the parameters found using the experimental data for the *big beam* dose contrast regime does not seem to give consistent results.
The next steps for this work would be to implement the RDE model into the RADDOSE-3D software to improve the DWD calculations. The recalculated DWD values can then be analysed with the global radiation damage figures for various crystals and we can establish whether the

DWD is a suitable dose statistic for faithfully representing global radiation damage.

# Appendices

## A Difference in FWHM of Convolved measurements and Deconvolved measurements

Since the FWHM is a function only of the standard deviation of the Gaussian distribution (FWHM $= 2\sigma\sqrt{2\ln(2)}$) then analysing the relationship between the FWHM of the convolved and deconvolved measurements is effectively equivalent to analysing the relationship between the standard deviations, $\sigma$ of the distributions. The equations for the one dimensional Gaussian function for the convolved and deconvolved data are

$$y_c = a_c \exp\left[-\frac{(x-\mu_c)^2}{2\sigma_c^2}\right], \tag{22}$$

$$y_d = a_d \exp\left[-\frac{(x-\mu_d)^2}{2\sigma_d^2}\right], \tag{23}$$

where the subscripts $c$ and $d$ correspond to the deconvolved and convolved parameters respectively, $y$ is the dependent variable, $x$ is the independent variable, $\mu$ is the mean of the distribution, $\sigma$ is the standard deviation of the distribution and $a$ is the maximum value of the distribution (i.e. $y = a$ when $x = \mu$). Rearranging equations 22 and 23 to make $\sigma^2$ the subject of the equation we get

$$\sigma_c^2 = -\frac{(x-\mu_c)^2}{2}\left[\frac{1}{\ln\left(\frac{y_c}{a_c}\right)}\right], \tag{24}$$

$$\sigma_d^2 = -\frac{(x-\mu_d)^2}{2}\left[\frac{1}{\ln\left(\frac{y_d}{a_d}\right)}\right]. \tag{25}$$

If we now subtract equation 25 from equation 24 we get

$$\sigma_c^2 - \sigma_d^2 = \frac{(x-\mu_d)^2}{2}\left[\frac{1}{\ln\left(\frac{y_d}{a_d}\right)}\right] - \frac{(x-\mu_c)^2}{2}\left[\frac{1}{\ln\left(\frac{y_c}{a_c}\right)}\right]. \tag{26}$$

If the FWHM of the convolved and deconvolved measurements are the same then equation 26 is equal to zero. This motivates investigation into the parameters more closely to see how close to zero this quantity is. First notice that in this case the convolution is the summation of all points within the aperture area (see Figure 12 for an illustration), hence the biggest value of the convolved data is going to occur where the biggest values of the deconvolved data are summed, and hence the maximum value occurs at the same position for both the deconvolved data and the convolved data. This implies that the mean for both sets of data are equivalent, more explicitly written, $\mu_d = \mu_c = \mu$. Substituting this into equation 26 and factorising we obtain

$$\sigma_c^2 - \sigma_d^2 = \frac{(x-\mu)^2}{2}\left[\frac{1}{\ln\left(\frac{y_d}{a_d}\right)} - \frac{1}{\ln\left(\frac{y_c}{a_c}\right)}\right]. \tag{27}$$

Equation 27 shows that the ratio between the dependent variable $y$ (in our case the flux) and the maximum value $a$ of the dependent variable for both the convolved and deconvolved data will determine the difference of the FWHM. Figure 12 gives the aperture set up in one dimension and hence shows how the flux measurements from the convolved data set relate to the flux measurements in the deconvolved data set (equation 28).

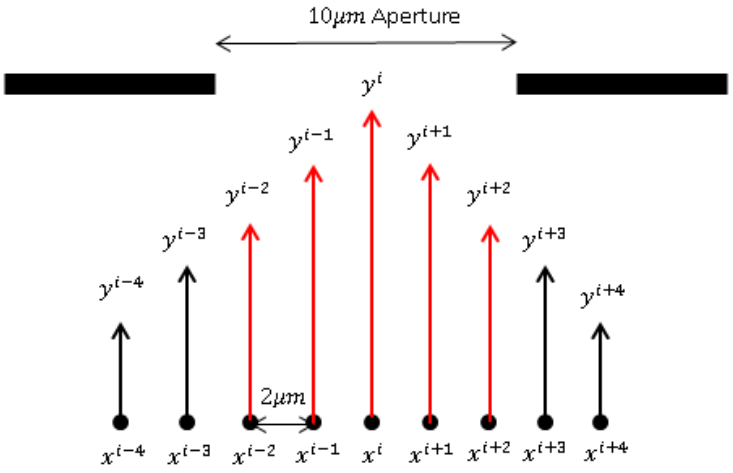


Figure 12: Diagram showing a model of the beam and aperture setup in one dimension. The red arrows correspond to the flux values that contribute to the flux readings at the point $x_i$. The aperture would then be moved by $2\mu m$ to the right and then another measurement is taken there.

$$y_c^i = y_d^{i-2} + y_d^{i-1} + y_d^i + y_d^{i+1} + y_d^{i+2}. \tag{28}$$

Equation 28 can also be written alternatively such that the right-hand side of the equation can be expressed in terms of the changes in the $y$ values where each consecutive change in $y$ is denoted by $\Delta y$. So equation 28 can alternatively be written as

$$y_c^i = (y_d^i - \Delta y^{i-2}) + (y_d^i - \Delta y^{i-1}) + y_d^i + (y_d^i + \Delta y^{i+1}) + (y_d^i + \Delta y^{i+2}). \tag{29}$$

Simplifying equation 29 we get

$$y_c^i = 5y_d^i + (\Delta y^{i+1} + \Delta y^{i+2} - \Delta y^{i-2} - \Delta y^{i-1}). \tag{30}$$

Using the symmetry of the Gaussian function it can be assumed that at the position of maximum flux (i.e. where $y_c^i = a_c$) the change in $y$ either side of the maximum is the same and hence the terms inside the brackets in equation 30 vanish (see Figure 12 for a pictorial representation of this assumption). This means that $a_c = 5a_d$ and hence equation 27 can be written as

$$\sigma_c^2 - \sigma_d^2 = \frac{(x-\mu)^2}{2}\left[\frac{1}{\ln\left(\frac{y_d}{a_d}\right)} - \frac{1}{\ln\left(\frac{y_c}{5a_d}\right)}\right]. \tag{31}$$

Equations 30 and 31 give information about the deviation in variances (and hence the FWHM) between the convolved and deconvolved data. Notice that for the left-hand side of equation 31 to vanish we require $y_c^i = 5y_d^i$. This means that the changes in $y$ either side of the point from which it is being measured need to be equal. This implies that for a complete top-hat beam, the width of the convolved and the deconvolved data sets should be the same (since there is no change in $y$ (i.e. flux) across the beam), but for a Gaussian with an incredibly small FWHM the deviation in the FWHM of the two data sets will be large. This is why we observed the discrepancy of the FWHM more in the $y$ data set with the smaller FWHM then in the $x$ data set as seen in Table 1. Additionally a bigger aperture size results in a convolution with more than 5 points and hence takes into account more change in $y$. This would mean that using a bigger aperture is more likely to return a FWHM that deviates more from the true value of the FWHM of the beam.

# B Derivation of Maximum Likelihood Estimate for a Binomial Distribution

For a binomially distributed random variable the probability of $k$ successes in $n$ trials, where the probability of success is $p$, is given by

$$P(k; n, p) = \binom{n}{k} p^k (1-p)^{n-k}. \tag{32}$$

The likelihood function is proportional to the probability and is given by

$$L(p; n, k) \propto p^k (1-p)^{n-k}. \tag{33}$$

Note that the position of the arguments on the left-hand side have been exchanged to explicitly show that the probability of success $p$ is now our variable and that $n$ and $k$ are the parameters. The log-likelihood function can be obtained by taking the logarithm of both sides of equation 33

$$\ell(p; n, k) = \log\left(L(p; n, k)\right) = k \log(p) + (n-k) \log\left(1-p\right). \tag{34}$$

It can be shown that the value of $p$ that maximises the log-likelihood function also maximises the likelihood function. To find the value that maximises the value of equation 34 the derivative of the function is taken with respect to $p$ giving

$$\frac{\partial \ell}{\partial p}(p; n, k) = \frac{k}{p} - \frac{n-k}{1-p}. \tag{35}$$

Setting the left hand side equal to zero and rearranging for $p$ we get

$$0 = \frac{k}{p} - \frac{n-k}{1-p} \Rightarrow p = \frac{k}{n} \tag{36}$$

as required. This shows that the maximum likelihood estimate of the parameter of success $p$ for a binomial distribution is equal to the number of successful trials divided by the number of total trials $k/n$. This is intuitive because it shows that as the number of trials tends to infinity the ratio should converge to the true probability of success.

# References


[1] Colin C.F. Blake and David C. Phillips. Effects of x-irradiation on single crystals of myoglobin. *Proceedings of the Symposium on the Biological effects of Ionizing Radiation at the Molecular Level*, pages 183–191, 1962.

[2] Jan Drenth. *Principles of Protein X-Ray Crystallography*. Springer Advanced Texts in Chemistry. Springer-Verlag GmbH, 1999.

[3] Jan Drenth. Introduction to basic crystallography. *International Tables for Crystallography, volume F*, pages 45–63, 2012.

[4] Elspeth F Garman. Radiation damage in macromolecular crystallography: what is it and why should we care? *Acta Crystallographica Section D: Biological Crystallography*, 66(4):339–351, 2010.

[5] R.C. González and R.E. Woods. *Digital image processing*. Addison-Wesley world student series. Addison-Wesley, 1992.

[6] James M Holton. A beginner's guide to radiation damage. *Journal of Synchrotron Radiation*, 16(2):133–142, 2009.

[7] A.C. King, J. Billingham, and S.R. Otto. *Differential equations: linear, nonlinear, ordinary, partial*. Cambridge University Press, 2003.

[8] Ricardo Miguel Ferraz Leal, Gleb Bourenkov, Silvia Russi, and Alexander N Popov. A survey of global radiation damage to 15 different protein crystal types at room temperature: a new decay model. *Journal of Synchrotron Radiation*, 20(1):14–22, 2012.

[9] James W Murray, Elspeth F Garman, and Raimond BG Ravelli. X-ray absorption by macromolecular crystals: the effects of wavelength and crystal composition on absorbed dose. *Journal of Applied Crystallography*, 37(4):513–522, 2004.

[10] Colin Nave and Elspeth F Garman. Towards an understanding of radiation damage in cryocooled macromolecular crystals. *Journal of Synchrotron Radiation*, 12(3):257–260, 2005.

[11] Robin Leslie Owen, Enrique Rudiño-Piñera, and Elspeth F Garman. Experimental determination of the radiation dose limit for cryocooled protein crystals. *Proceedings of the National Academy of Sciences of the United States of America*, 103(13):4912–4917, 2006.

[12] Karthik S Paithankar, Robin Leslie Owen, and Elspeth F Garman. Absorbed dose calculations for macromolecular crystals: improvements to raddose. *Journal of Synchrotron Radiation*, 16(2):152–162, 2009.

[13] Alexander N Popov and Gleb P Bourenkov. Choice of data-collection parameters based on statistic modelling. *Acta Crystallographica Section D: Biological Crystallography*, 59(7):1145–1153, 2003.

[14] Robert J Southworth-Davies, Melissa A Medina, Ian Carmichael, and Elspeth F Garman. Observation of decreased radiation damage at higher dose rates in room temperature protein crystallography. *Structure*, 15(12):1531–1541, 2007.

[15] Oliver B Zeldin, Markus Gerstel, and Elspeth F Garman. Optimizing the spatial distribution of dose in x-ray macromolecular crystallography. *Journal of Synchrotron Radiation*, 20(1):0–0, 2012.

[16] Oliver B. Zeldin, Markus Gerstel, and Elspeth F. Garman. *RADDOSE-3D*: time- and space-resolved modelling of dose in macromolecular crystallography. *Journal of Applied Crystallography*, 46(4), Aug 2013.